Electronic Supplementary Material (ESI) for Inorganic Chemistry Frontiers.

Supporting Information

Boosting oxygen reduction of well-dispersed CoP/V$(PO_3)_3$ sites via geometric and electronic engineering for flexible Zn-air battery

Zuyang Luo,[a,1] Fengli Wei,[a,1] Junlin Gong,[a] Lixia Wang,[a] Zhiyang Huang,[a] Tayirjan Taylor Isimjan,[b,*] Xiulin Yang[a,*]

[a] *Guangxi Key Laboratory of Low Carbon Energy Materials, School of Chemistry and Pharmaceutical Sciences, Guangxi Normal University, Guilin 541004, Guangxi, China*

[b] *Saudi Arabia Basic Industries Corporation (SABIC) at King Abdullah University of Science and Technology (KAUST), Thuwal 23955-6900, Saudi Arabia*

[1] *These authors contributed equally.*

* *Corresponding authors.*

E-mail addresses: xlyang@gxnu.edu.cn (X. Yang); isimjant@sabic.com (T.T. Isimjan).

Experiment section

Synthesis of CoP/V$(PO_3)_3$@HCS

All reagents were purchased from Sigma-Aldrich and used without further purification. 1.2 mmol 2,4-dihydroxybenzoic acid (DA) and 0.5 mmol methenamine (HMT) were dissolved in 60 mL H_2O. Then, a 20 mL aqueous solution containing 0.24 mmol sodium oleate (SO) and 0.0075 mmol Pluronic P123 was added. After stirring, 0.1 mmol VCl_3 and 0.2 mmol $CoCl_2$ were added and stirred for 10 min, then transferred into a Teflon-lined stainless-steel autoclave and heated at 160 ℃ for 2 h (product noted: CoV@HCS). Afterward, the CoV@HCS were collected, washed, and dried at 80 ℃ under vacuum. The CoP/V$(PO_3)_3$@HCS was obtained by grinding with red P and heating at 1000 ℃ for 2 h under Ar (2 ℃ min^{-1}). Additionally, CoP/V$(PO_3)_3$@HCS-900 and CoP/V$(PO_3)_3$@HCS-1100 were synthesized under 900 and 1100 ℃. For comparison, the CoP@HCS, V$(PO_3)_3$@HCS, and HCS were synthesized without the addition of $CoCl_2$, VCl_3, and metals, respectively.

Assembly and test of aqueous ZAB

The performance test of ZAB was carried out on the LAND-BT2016A workstation. The catalyst was configured as ink and cast evenly on carbon paper as an air cathode, and polished zinc plate as anode. 6 M KOH + 0.2 M $Zn(CH_3COO)_2$ was used as electrolyte. For comparison, 20 wt% Pt/C was involved. During the stability experiment, the prepared catalyst and RuO_2 were mixed in a mass ratio of 1:1 to prepare the catalyst slurry as an air cathode using the same method as above. For comparison, Pt/C+RuO_2 was also tested under the same conditions.

Assembly and test of flexible ZAB

Polyvinyl alcohol (PVA, 5 g) was dissolved in 50 mL H_2O at 90 ℃ with stirring for 1.5 h for a gel polymer electrolyte. Afterward, a mixed solution of 18 M KOH and 0.2 M $Zn(CH_3COO)_2$ was prepared and poured into the above gel with stirring for 30 min to freeze at –20 °C to form the final electrolyte gel. Ultimately, this prepared gel, a piece of carbon load catalyst as an air cathode, and a polished zinc foil were assembled into flexible ZAB.

Electrochemical measurements

ORR electrochemical tests were conducted on CHI 760E electrochemical workstation with

a three-electrode system (reference electrode: Ag/AgCl electrode, auxiliary electrode: graphite rod). The rotating ring disk electrode (RRDE, diameter = 5.61 mm, PINE instruments, USA) and rotating disk electrode (RDE, diameter = 5 mm, PINE instruments, USA) loaded with catalyst ink were used as the working electrode. To form a well-distributed catalyst ink, 1 mg electrocatalyst was dispersed into a mixed solution (containing 100 μL isopropanol, 100 μL H_2O, and 5 μL 5 wt% Nafion). Afterward, 25 μL catalyst ink was pipetted onto the surface of RDE and RRDE, respectively, and dried naturally. The measured potential was converted to the RHE from the Nernst equation (Fig. S1):

$$E_{RHE} = E_{Ag/AgCl} + 0.059pH + 0.196$$

Cyclic voltammetry (CV) measurements were carried out in O_2 or N_2-saturated 0.1 M KOH solution with a scan rate of 50 mV s^{-1}. Linear sweep voltammetry (LSV) curves were obtained in O_2-saturated 0.1 M KOH at a sweep rate of 10 mV s^{-1} with various rotation speeds (400-2025 rpm) and the potential range from – 0.9 to 0.2 V. The stability measurements were performed by using chronoamperometry at a rotation speed of 1600 rpm. The Tafel slopes were given by the equation:[1]

$$\eta = b\ log(\frac{j}{j_0})$$

The number of electrons transferred (n) was determined in combination with the RDE test by the Koutechy-Levich (K-L) equation:[2]

$$\frac{1}{j} = \frac{1}{j_k} + \frac{1}{B\omega^{1/2}}$$

$$B = 0.62nFC_0v^{-1/6}D_0^{2/3}$$

Where j and j_k represent the measured and kinetic current density (mA cm^{-2}), respectively. ω is the angular velocity, n is the electron transfer number of O_2, F is the Faraday constant (F = 96485 C mol^{-1}), C_0 and D_0 are the bulk concentration (1.2×10^{-3} mol L^{-1}) and diffusion coefficient (1.9×10^{-5} cm^2 s^{-1}) of O_2 in 0.1 M KOH, v is the dynamic viscosity (0.01 cm^2 s^{-1}).

The percentage of H_2O_2 yield (%) and n during ORR were calculated in combination with the RRDE test according to the following equations:[3]

$$n = 4\frac{I_d}{I_d + I_r/N}$$

$$H_2O_2(\%) = 200\frac{I_r/N}{I_d + I_r/N}$$

Where I_d and I_r denote the disk and ring currents, respectively.

Materials characterization

The micromorphology of as-prepared catalysts was determined by using a scanning electron microscope (SEM, FEI Quanta 200) and transmission electron microscope (TEM, Talos F200S). Raman spectroscopy (Renishaw in Via Quotation) is used to analyze the degree of disorder and graphitization of all samples. The surface valence and composition of the catalyst are analyzed by X-ray photoelectron spectroscopy (XPS, ESCALAB 250Xi) and X-ray diffraction (XRD, Rigaku D/Max-3c). Metal contents were investigated by inductively coupled plasma mass spectroscopy (ICP-MS, PerkinElmer corporation, FLexar-NexION300X). Brunauer−Emmett−Teller (BET) specific surface areas and pore size distribution were performed on nitrogen adsorption-desorption apparatus(3H-2000PS4). The contact angle of water was tested by a contact angle meter (JC2000D, China).

Computational methods and details

Spin-polarized DFT calculations were performed using the Vienna ab initio simulation package (VASP).[4] The generalized gradient approximation proposed by Perdew-Burke-Ernzerhof (GGA-PBE) is selected for the exchange-correlation potential.[5] The pseudo-potential was described by the projector-augmented-wave (PAW) method.[6] The geometry optimization is performed until the Hellmann–Feynman force on each atom is smaller than 0.03 eV·Å^{-1}. The energy criterion is set to 10^{-5} eV in the iterative solution of the Kohn-Sham equation.

The ORR performance was explored under the theoretical framework developed by Nørskov et al.[7] Here, the associative mechanism and a four-electron pathway were considered, according to which the ORR elementary reactions are described as follows:[8, 9]

$$O_2^* + H_2O + e^- \rightarrow OOH^* + OH^- \quad (\Delta G_1)$$

$$OOH^* + e^- \rightarrow O^* + OH^- \quad (\Delta G_2)$$

$$O^* + H_2O + e^- \rightarrow OH^* + OH^- \quad (\Delta G_3)$$

$$OH^* + e^- \rightarrow * + OH^- \quad (\Delta G_4)$$

Where * represents an active site. OOH*, O*, and OH* are the active sites with OOH, O, and OH intermediate adsorption, respectively. The free energy of the intermediates is defined as:

$$\Delta G = \Delta E + \Delta ZPE - T\Delta S + \Delta G_{pH} + \Delta G_U$$

Where ΔE is the reaction energy of each step, obtained from DFT calculations; ΔZEP is the change of zero-point energies in the reactions; $T\Delta S$ is the entropy contribution at 300 K.

ΔG_U is the influence of applied potential, defined as:

$$\Delta G_U = - eU$$

Where U is the potential at the electrode and e is the transferred charge. For the small difference between the vibrational frequencies of the adsorbents on the surface, the ΔZPE and $T\Delta S$ were taken from the previous literature.[10]

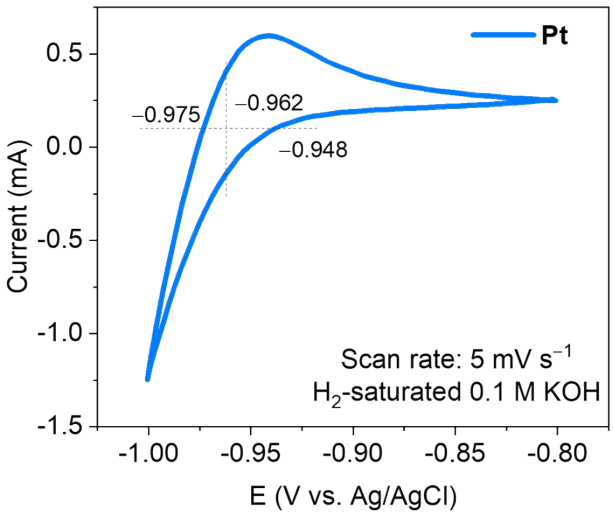

Fig. S1. RHE voltage calibration. CHI 760E electrochemical workstation calibration. the RHE calibration of saturated Ag/AgCl electrode in 0.1 M KOH. The average value of the potential at zero current is regarded as the thermodynamic potential for hydrogen electrode reaction, it is only 0.002 V away from the value calculated by the Nernst equation. The current-voltage scans were run at a scan rate of 5 mV s^{-1}, and the average of the two potentials at which the current crossed zero was taken to be the thermodynamic potential for the hydrogen electrode reactions.

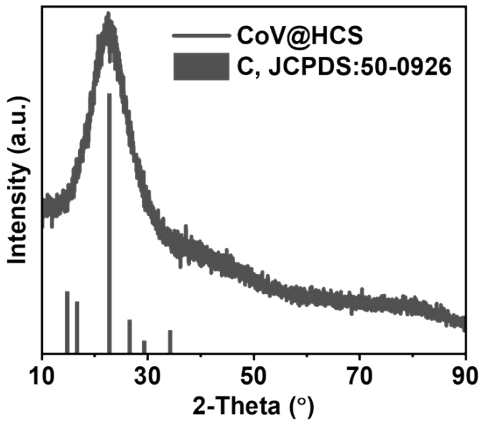

Fig. S2. XRD patterns of CoV@HCS.

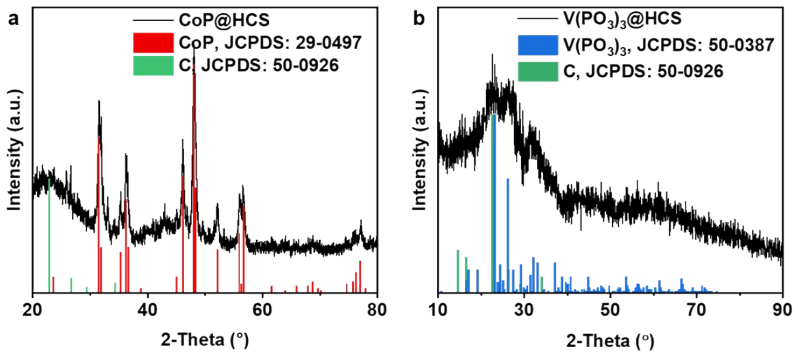

Fig. S3. XRD patterns of (a) CoP@HCS and (b) $V(PO_3)_3$@HCS.

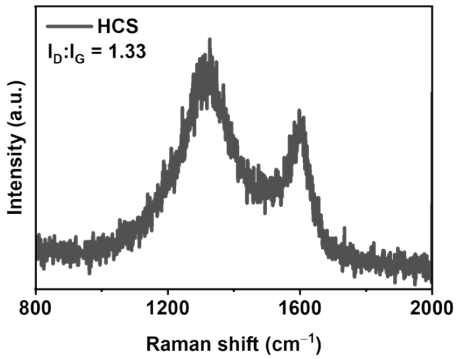

Fig. S4. Raman spectra of HCS.

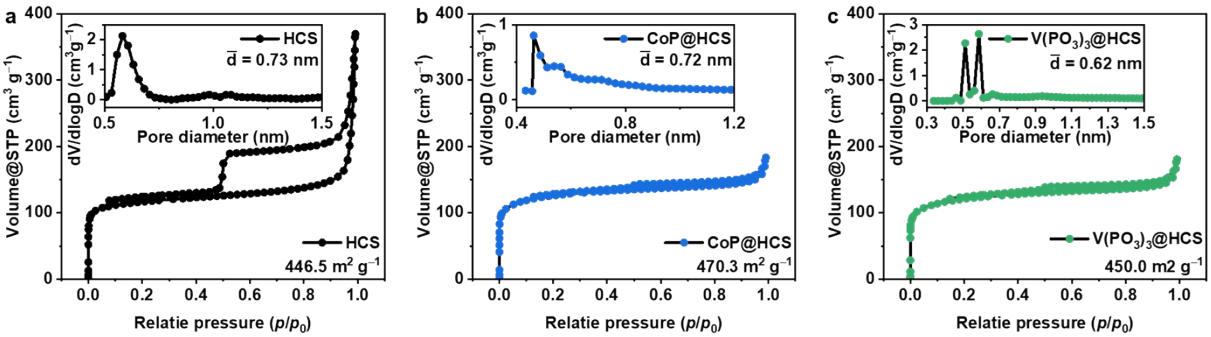

Fig. S5. N_2 des/adsorption isotherms of (a) HCS, (b) CoP@ HCS, and $V(PO_3)_3$@HCS (inset: corresponding pore size distribution).

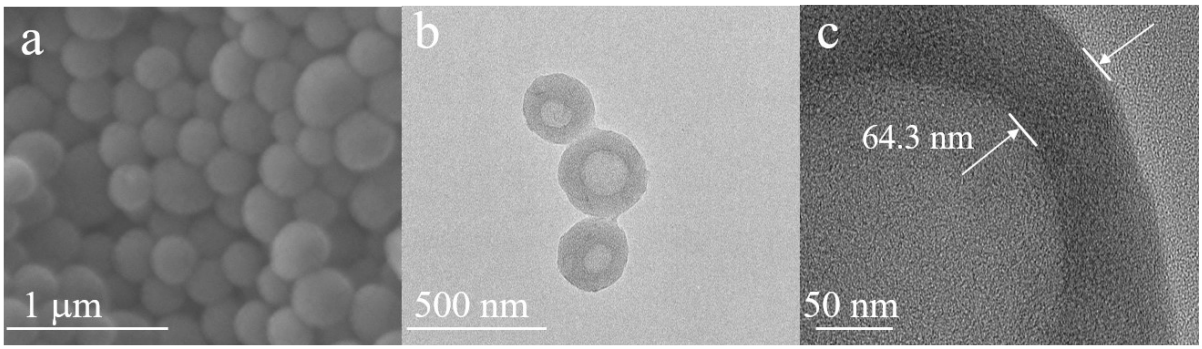

Fig. S6. (a) SEM, (b) TEM, and (c) HRTEM images of HCS.

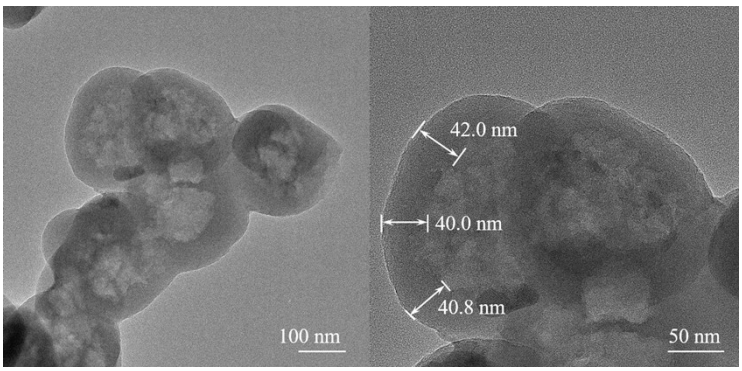

Fig. S7. (a) TEM and (b) HRTEM images of HCS.

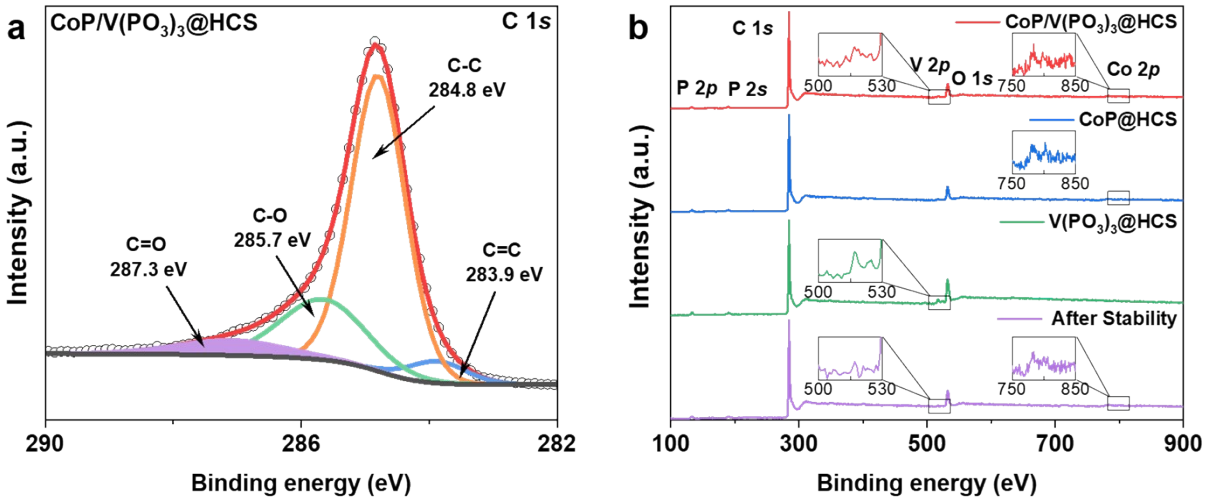

Fig. S8. (a) High-resolution XPS spectra of C 1*s* region of CoP/V$(PO_3)_3$@NC. (b) XPS survey spectra of CoP/V$(PO_3)_3$@NC, CoP@HCS, V$(PO_3)_3$@HCS and the sample after stability.

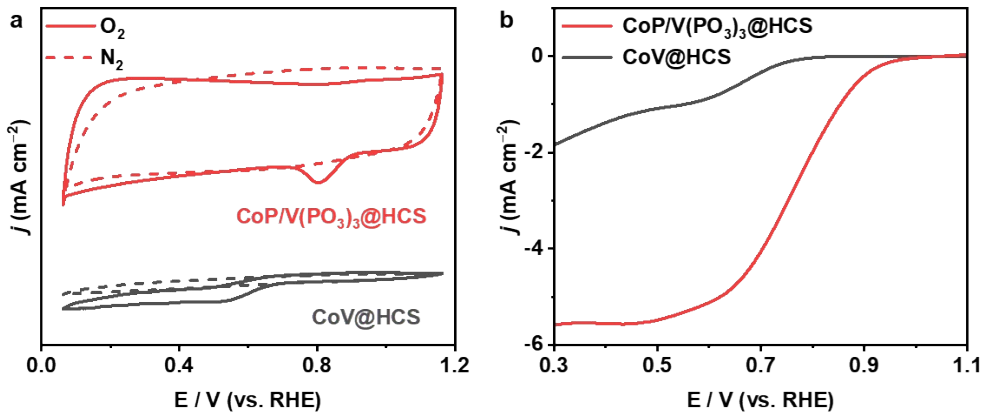

Fig. S9. (a) CV and (b) LSV polarization curves for CoP/V$(PO_3)_3$@HCS and CoV@HCS.

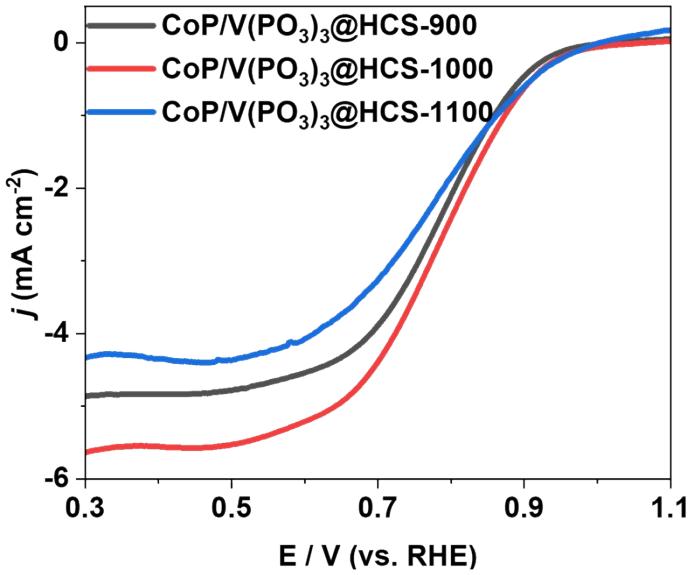

Fig. S10. LSV polarization curves for CoP/V$(PO_3)_3$@HCS-T (note: T is the different temperatures).

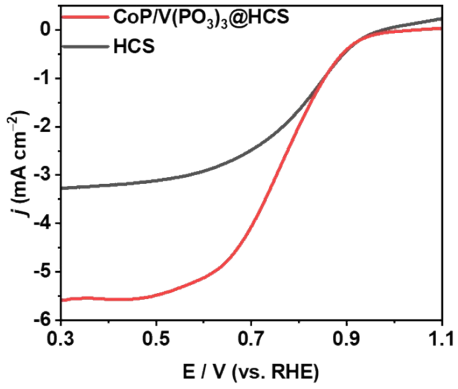

Fig. S11. LSV polarization curves for CoP/V$(PO_3)_3$@HCS and HCS.

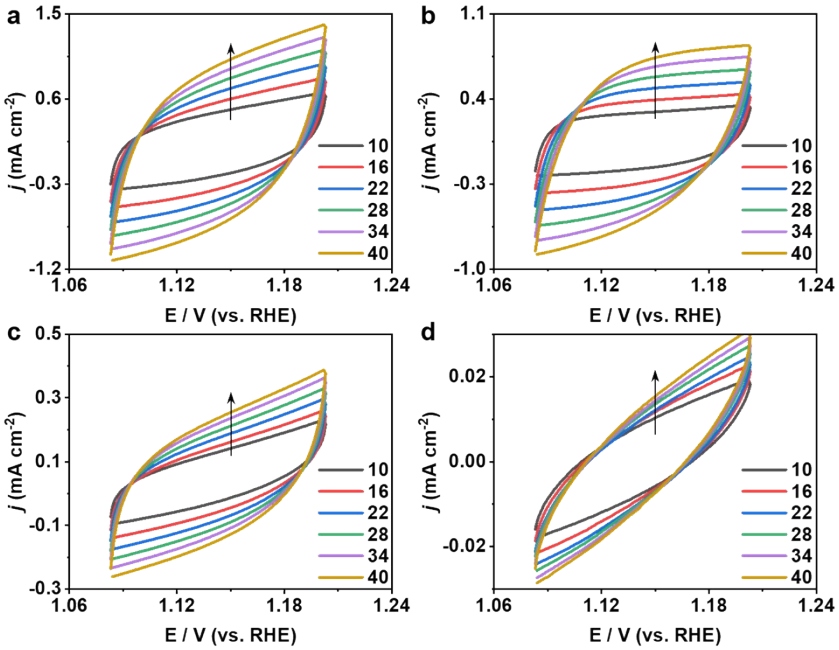

Fig. S12. CV curves of (a) CoP/V$(PO_3)_3$@HCS, (b) CoP@HCS, (c) V$(PO_3)_3$@HCS and (d) CoV@HCS at various scan rates in the non-Faradaic region.

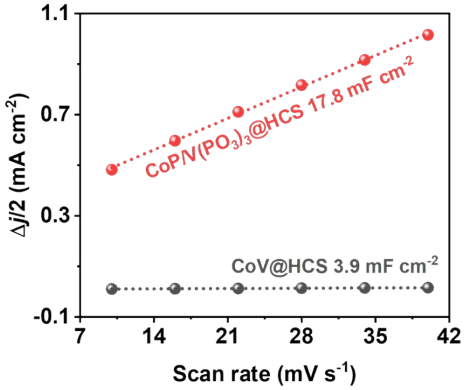

Fig. S13. C_{dl} values of CoP/V$(PO_3)_3$@HCS and CoV@HCS.

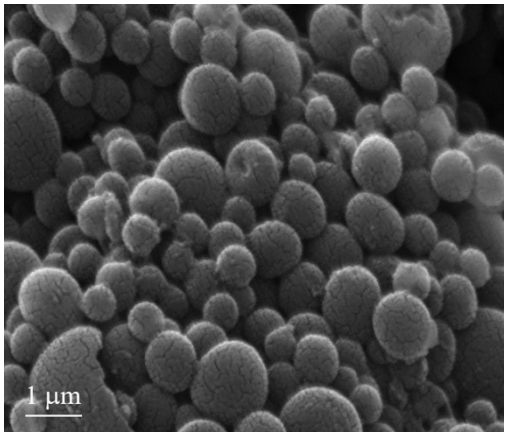

Fig. S14. SEM of CoP/V$(PO_3)_3$@HCS after stability.

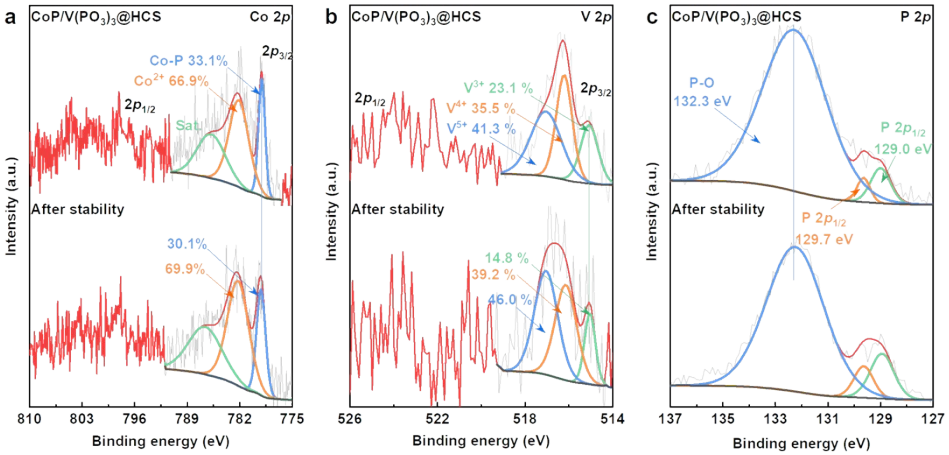

Fig. S15. High-resolution XPS spectra of (a) Co 2*p*, (b) V 2*p*, and (c) P 2*p* for CoP/V$(PO_3)_3$@HCS before and after stability.

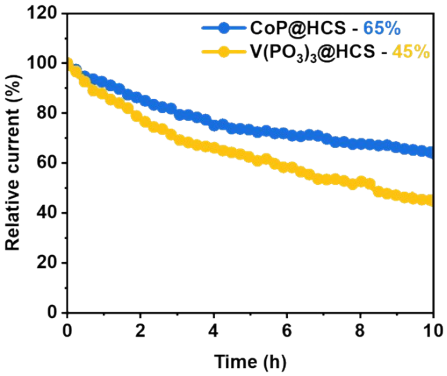

Fig. S16. Chronoamperometric (CP) response of CoP@HCS and $V(PO_3)_3$@HCS.

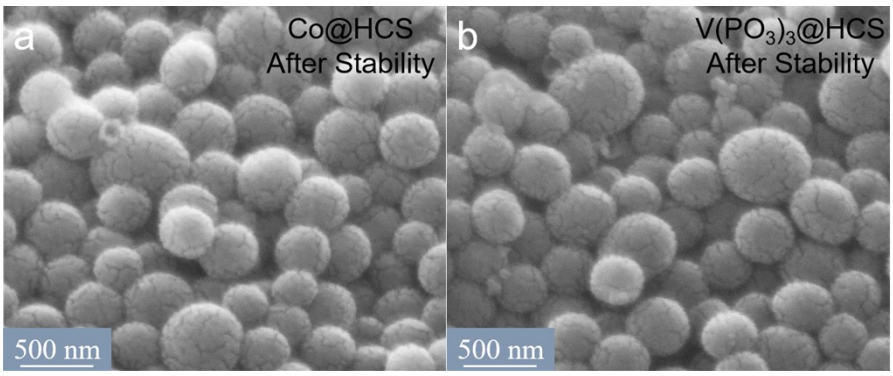

Fig. S17. SEM images of CoP@HCS and $V(PO_3)_3$@HCS after stability.

Table S1. The metal content of the as-prepared samples according to inductively coupled plasma mass spectroscopy (ICP-MS) results.

Catalyst	Co (wt.%)	V (wt.%)
CoP/$V(PO_3)_3$@NC	22.4	3.6
CoP@NC	17.3	--
$V(PO_3)_3$@NC	--	7.3

Table S2. Comparison of CoP/V$(PO_3)_3$@NC with currently reported ORR electrocatalysts in 0.1 M KOH solution.

Catalysts	Tafel slope (mV dec^{-1})	j_L (mA cm^{-2})	Reference
CoP/V$(VPO_3)_3$@HCS	**79.2**	**5.6**	**This work**
Pt/C	86.5	4.9	This work
Co SAs/NPs	89.1	6.1	[11]
FeN_x/C-700-20	93.0	5.7	[12]
Ru-FeRu@C/NC	99.3	5.2	[13]
Fe_2O_3/Fe_5C_2/Fe–N–C	86.5	4.8	[14]
NSC	112.4	5.4	[15]
Co_3P/C	82.5	3.5	[16]
Fe/NC	90.2	5.3	[17]
Fe@NWC	109.1	4.9	[18]
Fe/NC CNFs	98.2	4	[19]
LSTFO-H	95.0	5.3	[20]
CoP	95.7	6.2	[21]
BCN/rGO-Co	70.5	5.4	[22]
Co/NC	91.1	5.4	[15]
FeCoP/C	55.0	5.1	[23]
FePc&rGO	39.1	5.4	[24]
COP_{BTC}	143.0	4.5	[25]
N-G NSs	66.0	5.2	[26]

Table S3. Comparison of $CoP/V(PO_3)_3$@NC-based ZABs with currently reported ZABs.

Catalysts	Open-circuit voltage (V)	Power density (mW cm^{-2})	Charge-discharge cycle stability (h)	Electrolyte	Reference
$CoP/V(PO_3)_3$@HCS	**1.56**	**182**	**710**	**6 M KOH + 0.2 M $Zn(CH_3COO)_2$**	**This work**
Cu/Cu_3P@NP-C-900	1.42	148	300	6 M KOH + 0.2 M $Zn(CH_3COO)_2$	27
WC/Co_7Fe_3-NPHC	1.43	270	550	6 M KOH + 0.2 M $Zn(CH_3COO)_2$	28
Co_2P/Co-N-C	1.50	158	205	6 M KOH + 0.2 M $Zn(CH_3COO)_2$	29
Co_xP-NC-420	1.37	54	100	6 M KOH + 0.2 M $Zn(CH_3COO)_2$	30
Ni_2P/CNTs	1.42	153		6 M KOH + 0.2 M $Zn(CH_3COO)_2$	31
NCFPO-350	1.35	75	30	6 M KOH + 0.2 M $Zn(CH_3COO)_2$	32
NiFe(1:2)P/Pi	1.45	395	100	6 M KOH + 0.2 M $Zn(CH_3COO)_2$	33
CNCP-450		178	50	6 M KOH + 0.2 M $Zn(CH_3COO)_2$	34
FeCoP/C	1.39	115	100	6 M KOH + 0.2 M $Zn(CH_3COO)_2$	23
Co-FPOH	1.42	167	450	6 M KOH + 0.2 M $Zn(CH_3COO)_2$	35
Co/VN NPs@C	1.41	130	600	6 M KOH + 0.2 M $Zn(CH_3COO)_2$	36
Co@IC/MoC@PC	1.48	252	100	6 M KOH + 0.2 M $Zn(CH_3COO)_2$	37
LZAB@Co-SAs/N–C/rGO	1.52	105		6 M KOH + 0.2 M $Zn(CH_3COO)_2$	38
BCN/rGO-Co	1.46	157	200	6 M KOH + 0.2 M $Zn(CH_3COO)_2$	22
CNT@SAC-Co/NCP	1.45	172	34	6 M KOH + 0.2 M $Zn(CH_3COO)_2$	39
ZAB-Fe_3Co_7-NC	1.52	133	400	6 M KOH + 0.2 M $Zn(CH_3COO)_2$	40
V-KFO/NF	1.29	140	550	6.0 M KOH + 0.02 M $Zn(CH_3COO)_2$	41
$Mn_x(PO_4)_y$/NPC	1.27		34	6.0 M KOH + 0.02 M $Zn(CH_3COO)_2$	42

$CuNi_2$-S/G	1.32	127	210	6 M KOH + 0.2 M $Zn(CH_3COO)_2$	43
N-HPCs	1.41	158	100	6 M KOH + 0.2 M $Zn(CH_3COO)_2$	26
Co_3O_4@Ni_2P	1.33	184	177	6 M KOH + 0.2 M $Zn(CH_3COO)_2$	44
$S_{0.95}$NCF-600	1.46		500	6 M KOH + 0.2 M $Zn(CH_3COO)_2$	45
CoP/CoO@MNC-CN	1.42	153	500	6 M KOH + 0.2 M $Zn(CH_3COO)_2$	1
FeCo@CoN_x@FeP_x/C	1.45	110	700	6 M KOH + 0.2 M $Zn(CH_3COO)_2$	46
Pt@CoN_4-G	1.50	316		6 M KOH + 0.2 M $Zn(CH_3COO)_2$	47
FeNi/Co_4N-NCS-zab	1.57	160	1450	6 M KOH + 0.2 M $Zn(CH_3COO)_2$	48
ES-Co/Zn-CNZIF	1.53	215	254	6 M KOH + 0.2 M $Zn(CH_3COO)_2$	49
SC-Cu_{SA}-NC	1.49	125	120	6 M KOH + 0.2 M $Zn(CH_3COO)_2$	50
CoSA-RuO_2- NUCN	1.55	157	800	6 M KOH + 0.2 M $Zn(CH_3COO)_2$	51
Fe/Cu-N-C	1.48	183	140	6 M KOH + 0.2 M $Zn(CH_3COO)_2$	52
Co SAs/NPs CNF	1.43	152	450	6 M KOH + 0.2 M $Zn(CH_3COO)_2$	11
Ni-SAs/HCNFs/Co-NAs	1.45	140.7	220	18M KOH + 0.02 M $Zn(CH_3COO)_2$	53
Fe–N–C/Fe_3C-op	1.56	137.4	450	6 M KOH + 0.2 M $Zn(CH_3COO)_2$	54

References

1. H. W. Go, T. T. Nguyen, Q. P. Ngo, R. Chu, N. H. Kim and J. H. Lee, Tailored heterojunction active sites for oxygen electrocatalyst promotion in zinc-air batteries, *Small*, 2023, **19**, 2206341.

2. C. Hu, Q. Liang, Y. Yang, Q. Peng, Z. Luo, J. Dong, T. T. Isimjan and X. Yang, Conductivity-enhanced porous N/P co-doped metal-free carbon significantly enhances oxygen reduction kinetics for aqueous/flexible zinc-air batteries, *J. Colloid Interface Sci.* , 2023, **633**, 500.

3. C. Hu, F. Wei, Q. Liang, Q. Peng, Y. Yang, T. Taylor Isimjan and X. Yang, Electronically

modulated d-band centers of MOF-derived carbon-supported Ru/HfO_2 for oxygen reduction and aqueous/flexible zinc-air batteries, *J. Energy Chem.*, 2023, **80**, 247.
4. G. Kresse a and J. Furthmüller, Efficiency of ab-initio total energy calculations for metals and semiconductors using a plane-wave basis set, *Mater. Sci.*, 1996, **6**, 15.
5. J. P. Perdew, K. Burke and M. Ernzerhof, Generalized Gradient Approximation Made Simple, *Phy. Rev. Lett.*, 1996, **77**, 3865.
6. P. E. Blochl, Projector augmented-wave method, *Phys. Rev. B*, 1994, **50**, 17953.
7. J. K. Nørskov, J. Rossmeisl, A. Logadottir, L. Lindqvist, J. R. Kitchin, T. Bligaard and H. Jónsson, Origin of the Overpotential for Oxygen Reduction at a Fuel-Cell Cathode, *J. Phys. Chem. B*, 2004, **108**, 17886.
8. K. Wan, T. Chu, B. Li, P. Ming and C. Zhang, Rational design of atomically dispersed metal site electrocatalysts for oxygen reduction reaction, *Adv. Sci.*, 2023, **20**, 2203391.
9. W. Xue, Q. Zhou, X. Cui, J. Zhang, S. Zuo, F. Mo, J. Jiang, X. Zhu and Z. Lin, Atomically Dispersed FeN_2 P_2 Motif with High Activity and Stability for Oxygen Reduction Reaction Over the Entire pH Range, *Angew. Chem. Int. Ed.*, 2023, **62**, e202307504.
10. J. Rossmeisl, Z. W. Qu, H. Zhu, G. J. Kroes and J. K. Nørskov, Electrolysis of water on oxide surfaces, *J. Electroanal. Chem.*, 2007, **607**, 83.
11. Y. Cheng, H. Song, J. Yu, J. Chang, G. I. N. Waterhouse, Z. Tang, B. Yang and S. Lu, Carbon dots-derived carbon nanoflowers decorated with cobalt single atoms and nanoparticles as efficient electrocatalysts for oxygen reduction, *Chin. J. Catal.*, 2022, **43**, 2443.
12. S. Han, X. Hu, J. Wang, X. Fang and Y. Zhu, Novel Route to Fe-Based Cathode as an Efficient Bifunctional Catalysts for Rechargeable Zn-Air Battery, *Adv. Energy Mater.* , 2018, **8**, 1800955.
13. W. Feng, Y. Feng, J. Chen, H. Wang, Y. Hu, T. Luo, C. Yuan, L. Cao, L. Feng and J. Huang, Interfacial electronic engineering of Ru/FeRu nanoparticles as efficient trifunctional electrocatalyst for overall water splitting and Zn-air battery, *Chem. Eng. J.* , 2022, **437**, 135456.
14. X. Guo, S. Liu, X. Wan, J. Zhang, Y. Liu, X. Zheng, Q. Kong and Z. Jin, Controllable solid-phase fabrication of an Fe_2O_3/Fe_5C_2/Fe-N-C electrocatalyst toward optimizing the oxygen reduction reaction in zinc-air batteries, *Nano Lett.*, 2022, **22**, 4879.
15. W. Li, J. Wang, J. Chen, K. Chen, Z. Wen and A. Huang, Core-shell carbon-based bifunctional electrocatalysts derived from COF@MOF hybrid for advanced rechargeable Zn-air batteries, *Small*, 2022, **18**, 2202018.
16. J. Li, Y. Kang, Z. Lei and P. Liu, Well-controlled 3D flower-like CoP_3/CeO_2/C heterostructures as bifunctional oxygen electrocatalysts for rechargeable Zn-air batteries, *Appl. Catal. B Environ.*, 2023, **321**, 122029.
17. S. Ji, T. Liu, L. Leng, H. Liu, J. Zhang, M. Zhang, Q. Xu, J. Zhu, M. Qiao, Y. Wang, J. H. Horton and Z. Li, Protein-mediated synthesis of iron single atom electrocatalyst with highly accessible active sites for enhanced pH-universal oxygen reduction, *Appl. Catal. B Environ.*,

2023, **320**, 121987.
18. Y. Wang, Y. Liu, L. Zhou, P. Zhang, X. Wu, T. Liu, S. Mehdi, X. Guo, J. Jiang and B. Li, $Ni_3Fe/Ni_3Fe(OOH)_x$ dynamically coupled on wood-derived nitrogen doped carbon as a bifunctional electrocatalyst for rechargeable zinc–air batteries, *J. Mater. Chem. A*, 2023, **11**, 1894.
19. X. Chen, J. Pu, X. Hu, L. An, J. Jiang and Y. Li, Confinement synthesis of bimetallic MOF-derived defect-rich nanofiber electrocatalysts for rechargeable Zn-air battery, *Nano Res.*, 2022, **15**, 9000.
20. F. Li, N. Mushtaq, T. Su, Y. Cui, J. Huang, M. Sun, M. Singh, X. Zhao, K. Maliutina, Y. Zhang, C. He, M. Yang, B. Zhu and L. Fan, NCNT grafted perovskite oxide as an active bifunctional electrocatalyst for rechargeable zinc-air battery, *Mater. Today Nano*, 2023, **21**, 100287.
21. L. H. Xu, W. J. Wang, X. J. Zhang, S. Cosnier, R. S. Marks and D. Shan, Regulating the coordination capacity of ATMP using melamine: facile synthesis of cobalt phosphides as bifunctional electrocatalysts for the ORR and HER, *Nanoscale*, 2022, **14**, 17995.
22. L. Cao, Y. Wang, Q. Zhu, L. Fan, Y. Wu, Z. Li, S. Xiong and F. Gu, Co/Co-N/Co-O Rooted on rGO Hybrid BCN Nanotube Arrays as Efficient Oxygen Electrocatalyst for Zn-Air Batteries, *ACS Appl. Mater. Interfaces*, 2022, **14**, 17249.
23. R. Zhao, B. Ni, L. Wu, P. Sun and T. Chen, Carbon-based iron-cobalt phosphate FeCoP/C as an effective ORR/OER/HER trifunctional electrocatalyst, *Colloids Surf. A Physicochem. Eng. Aspects*, 2022, **635**, 128118.
24. Z.-y. Mei, S. Cai, G. Zhao, Q. Jing, X. Sheng, J. Jiang and H. Guo, Understanding electronic configurarions and coordination environment for enhanced ORR process and improved Zn-air battery performance, *Energy Storage Mater.*, 2022, **50**, 12.
25. X. Li, Q. Liu, B. Yang, Z. Liao, W. Yan and Z. Xiang, An Initial Covalent Organic Polymer with Closed-F Edges Directly for Proton-Exchange-Membrane Fuel Cells, *Adv. Mater.*, 2022, **34**, 2204570.
26. F. Kong, X. Cui, Y. Huang, H. Yao, Y. Chen, H. Tian, G. Meng, C. Chen, Z. Chang and J. Shi, N-Doped carbon electrocatalyst: marked ORR activity in acidic media without the contribution from metal sites?, *Angew. Chem. Int. Ed.*, 2022, **61**, 202116290.
27. Y. Huang, F. Kong, F. Pei, L. Wang, X. Cui and J. Shi, Modulating the electronic structure of hollow Cu/Cu_3P hetero-nanoparticles to boost the oxygen reduction performance in long-lasting Zn-air battery, *EcoMat*, 2023, **5**, 12335.
28. H. Mao, X. Liu, S. Wu, Y. Fu, G. Liu, G. Zhou and L. Wang, WC/Co_7Fe_3 heterojunction embedded in N,P co-doped hierarchical carbon enables rechargeable/flexible Zn-air battery, *Nano Res.*, 2022, **16**, 2519.
29. Q. Xu, X. Peng, Z. Zhu, K. Luo, Y. Liu and D. Yuan, Co_2P nanoparticles supported on cobalt-embedded N-doped carbon materials as a bifunctional electrocatalyst for rechargeable

Zn-air batteries, *Int. J. Hydrogen Energy*, 2022, **47**, 16518.
30. L. Bo, W. Liu, R. Liu, Y. Hu, L. Pu, F. Nian, Z. Zhang, P. Li and J. Tong, CoP/Co_2P hollow spheres embedded in porous N-doped carbon as highly efficient multifunctional electrocatalyst for Zn–air battery driving water splitting device, *Electrochim. Acta*, 2022, **403**, 139643.
31. K. Ma, R. Guo, J. Wang, X. Li, M. Ma and M. Sheng, Ni_2P nanoparticles encapsulated in carbon nanotubes as high-performance electrocatalyst for rechargeable zinc-air battery, *Mater. Lett.*, 2023, **333**, 133665.
32. D.-S. Pan, P. Chen, L.-L. Zhou, J.-H. Liu, Z.-H. Guo and J.-L. Song, Self-template construction of 2D amorphous N-doped CoFe-mesoporous phosphate microsheets for zinc-air batteries, *J. Power Sources*, 2021, **498**, 229859.
33. N. Thakur, M. Kumar, D. Mandal and T. C. Nagaiah, Nickel Iron Phosphide/Phosphate as an Oxygen Bifunctional Electrocatalyst for High-Power-Density Rechargeable Zn-Air Batteries, *ACS Appl. Mater. Interfaces*, 2021, **13**, 52487.
34. Z.-H. Guo, C. Yue, K.-Q. Ou, L.-F. Wu, Q.-Y. Lv, J.-Y. Lin, P.-R. Chen, J.-H. Liu, S. Huang, J.-K. Li and J.-L. Song, Amorphous C,N Codoping Cobalt Phosphates Simply Fabricated via a Mild Host–Guest Strategy as Bifunctional Electrocatalysts for Zinc–Air Batteries, *Energy Technol.*, 2021, **10**, 2100940.
35. L. Song, T. Zheng, L. Zheng, B. Lu, H. Chen, Q. He, W. Zheng, Y. Hou, J. Lian, Y. Wu, J. Chen, Z. Ye and J. Lu, Cobalt-doped basic iron phosphate as bifunctional electrocatalyst for long-life and high-power-density rechargeable zinc-air batteries, *Appl. Catal. B Environ.*, 2022, **300**, 120712.
36. H. Zheng, N. Xu, B. Hou, X. Zhao, M. Dong, C. Sun, X. L. Wang and Z. M. Su, Bimetallic Metal-Organic Framework-Derived Graphitic Carbon-Coated Small Co/VN Nanoparticles as Advanced Trifunctional Electrocatalysts, *ACS Appl. Mater. Interfaces*, 2021, **13**, 2462.
37. L. Zhang, Y. Zhu, Z. Nie, Z. Li, Y. Ye, L. Li, J. Hong, Z. Bi, Y. Zhou and G. Hu, Co/MoC Nanoparticles Embedded in Carbon Nanoboxes as Robust Trifunctional Electrocatalysts for a Zn-Air Battery and Water Electrocatalysis, *ACS Nano*, 2021, **15**, 13399.
38. L. Li, N. Li, J. Xia, S. Zhou, X. Qian, F. Yin, G. He and H. Chen, Metal–organic framework-derived Co single atoms anchored on N-doped hierarchically porous carbon as a pH-universal ORR electrocatalyst for Zn–air batteries, *J. Mater. Chem. A*, 2023, **11**, 2291.
39. J. C. Li, Y. Meng, L. Zhang, G. Li, Z. Shi, P. X. Hou, C. Liu, H. M. Cheng and M. Shao, Dual-Phasic Carbon with Co Single Atoms and Nanoparticles as a Bifunctional Oxygen Electrocatalyst for Rechargeable Zn–Air Batteries, *Adv. Funct. Mater.*, 2021, **31**, 2103360.
40. T. Gu, D. Zhang, Y. Yang, C. Peng, D. Xue, C. Zhi, M. Zhu and J. Liu, Dual-sites coordination engineering of single atom catalysts for full-temperature adaptive flexible ultralong-life solid-state Zn−air batteries, *Adv. Funct. Mater.*, 2022, **33**, 2212299.
41. J. Jian, P. Nie, Z. Wang, Y. Qiao, H. Wang, C. Zhang, X. Xue, L. Fang and L. Chang, V^{5+}-

Doped Potassium Ferrite as an Efficient Trifunctional Catalyst for Large-Current-Density Water Splitting and Long-Life Rechargeable Zn-Air Battery, *ACS Appl. Mater. Interfaces*, 2022, **14**, 36721.

42. S. Wang, G. Nam, P. Li, H. Jang, J. Wang, M. G. Kim, Z. Wu, X. Liu and J. Cho, $Mn_x(PO_4)_y$/NPC as a high performance bifunctional electrocatalyst for oxygen electrode reactions, *ChemCatChem*, 2019, **11**, 1222.

43. Z. Wang, X. Liao, M. Zhou, F. Huang, K. A. Owusu, J. Li, Z. Lin, Q. Sun, X. Hong, C. Sun, Y. B. Cheng, Y. Zhao and L. Mai, Interfacial and Vacancies Engineering of Copper Nickel Sulfide for Enhanced Oxygen Reduction and Alcohols Oxidation Activity, *Energy Environ. Mater.*, 2023, **6**, e12409.

44. X. Hu, T. Yang, Z. Yang, Z. Li, R. Wang, M. Li, G. Huang, B. Jiang, C. Xu and F. Pan, Engineering of Co_3O_4@Ni_2P heterostructure as trifunctional electrocatalysts for rechargeable zinc-air battery and self-powered overall water splitting, *J. Mater. Sci. Technol.*, 2022, **115**, 19.

45. S. Kim, J.-W. Jung, D. Song, S.-H. Cho, J. Kim, J. K. Kim, D. Oh, H. Sun, E. Cho, I.-D. Kim and W. Jung, Exceptionally durable CoFe-exsolved $Sr_{0.95}Nb_{0.1}Co_{0.7}Fe_{0.2}O_3$–δ catalyst for rechargeable Zn–air batteries, *Appl. Catal. B Environ.*, 2022, **315**, 121553.

46. W. Ding, A. Saad, Y. Wu, Z. Wang and X. Li, CNTs/CNF-supported multi-active components as highly efficient bifunctional oxygen electrocatalysts and their applications in zinc-air batteries, *Nano Res.*, 2023, **16**, 4793.

47. M. Zhang, H. Li, J. Chen, F. X. Ma, L. Zhen, Z. Wen and C. Y. Xu, A Low-Cost, Durable Bifunctional Electrocatalyst Containing Atomic Co and Pt Species for Flow Alkali-Al/Acid Hybrid Fuel Cell and Zn–Air Battery, *Adv. Funct. Mater.*, 2023, DOI: 10.1002/adfm.202303189, 10.1002/adfm.202303189.

48. W. Xie, Y. Liu, Y. Yan, M. Yang, M. Zhang, B. Liu, H. Li, H. Chen and Z. Lin, Metal-mediated Schiff base polymer enables metal/nitrogen codoped carbon nanosheets as efficient bifunctional electrocatalyst for durable rechargeable Zn-air batteries, *Energy Storage Mater.*, 2023, **59**, 102783.

49. Y. Ma, S. Tang, H. Wang, Y. Liang, D. Zhang, X. Xu, Q. Wang and W. Li, Bimetallic ZIFs-derived electrospun carbon nanofiber membrane as bifunctional oxygen electrocatalyst for rechargeable zinc-air battery, *J. Energy Chem.*, 2023, **83**, 138.

50. Y. Zhang, L. Chen, B. Yan, F. Zhang, Y. Shi and X. Guo, Single Cu atoms confined in N-doped porous carbon networks by flash nanocomplexation as efficient trifunctional electrocatalysts for Zn-air batteries and water splitting, *Compos. Part B Eng.*, 2023, **253**, 110575.

51. X. Ma, M. Liu, Q. Li, X. Xiao, J. Liu, X. Xu, Y. Yin, P. Qiao, L. Zhang, X. Zou, R. Wang and B. Jiang, Associating Co single atoms with RuO_2 nanoparticles anchor on nitrogen-doped ultrathin porous carbon nanosheets as effective bifunctional oxygen electrocatalysts for rechargeable Zn–air batteries, *J. Mater. Chem. A.*, 2023, **11**, 16889.

52. M. Bu, Y. Liu, S. Liao, W. Liu, Z. Yang, J. Jiang, X. Gao, Y. Yang and H. Liu, In-site grown carbon nanotubes connecting Fe/Cu-N-C polyhedrons as robust electrocatalysts for Zn-air batteries, *Carbon*, 2023, **214**, 118365.
53. Y. Chen, S. Qiao, Y. Tang, Y. Du, D. Zhang, W. Wang, H. Zhang, X. Sun and C. Liu, Double-faced atomic-level engineering of hollow carbon nanofibers as free-standing bifunctional oxygen electrocatalysts for flexible Zn–air battery, *ACS Nano*, 2022, **16**, 15273.
54. J. Chang, Q. Zhang, J. Yu, W. Jing, S. Wang, G. Yin, G. I. N. Waterhouse and S. Lu, A Fe single atom seed-mediated strategy toward Fe_3C/Fe-N-C catalysts with outstanding bifunctional ORR/OER activities, *Adv. Sci.*, 2023, **10**, 2301656.